Physics of Fluids

RESEARCH ARTICLE | MAY 03 2023

Launching phenomenon of a centimeter-scale solid object using explosive boiling due to electrical discharge in water

Hideyuki Sugioka ; Katsuaki Murata ; Yuki Arai

Physics of Fluids 35, 054105 (2023)
https://doi.org/10.1063/5.0143832

Physics of Fluids ARTICLE scitation.org/journal/phf

Launching phenomenon of a centimeter-scale solid object using explosive boiling due to electrical discharge in water

Cite as: Phys. Fluids **35**, 054105 (2023); doi: 10.1063/5.0143832
Submitted: 26 January 2023 · Accepted: 18 April 2023 ·
Published Online: 3 May 2023

Hideyuki Sugioka,[a] Katsuaki Murata, and Yuki Arai

AFFILIATIONS

Department of Mechanical Systems Engineering, Shinshu University, 4-17-1 Wakasato, Nagano 380-8553, Japan

[a]Author to whom correspondence should be addressed: hsugioka@shinshu-u.ac.jp

ABSTRACT

Technology to launch objects into the air is essential for various applications. In this study, we propose a solid object launcher that pushes the object of centimeter-scale by the rapid liquid motion resulting from explosive vaporization due to electric discharge in water. In particular, by using the electric discharge in a trapezoid-shaped chamber, we demonstrate that a centimeter-scale L-shaped piece of paper with 0.92 mg mass can be launched with an initial velocity ∼4 m/s in the direction of an elevation angle of ∼50°, while a centimeter-scale paper airplane with 29.6 mg mass can be launched with the maximum velocity ∼2 m/s along a glass slide runway with an elevation angle of ∼45°. In addition, to clarify the mechanism of solid launching phenomena, we systematically carried out vertical launching experiments of the centimeter-scale solid object of 60–340 mg. Moreover, as a central design concept peculiar to the solid launching device, we demonstrate the importance of water-repellent treatment of the solid surface. In the future, our device might be used to provide object-shooting technology for hybrid manufacturing technology or to protect orchards from birds.

I. INTRODUCTION

Technology to launch objects into the air is essential for various applications, e.g., rockets, airplanes, drones, micro-aerial vehicles (MAVs),[1,2] seed ejection of plants,[3] 3D-printers,[4] painting, inkjet printing,[5] and plasma sprays.[6] In particular, micro-thermal liquid ejectors using strong vaporization (boiling) phenomena have attracted much attention and are widely used commercially. Here, boiling phenomena are attractive as a driving force because of the ability to produce large mechanical work due to latent heat energy.[7–11] Furthermore, thermal liquid ejector[7,12] is a device that ejects a liquid (ink) droplet using a film boiling phenomenon[13,14] on a thin film heater. Because of their practical and scientific importance, various studies have been devoted to this issue so far.[7,15–18] For example, Asai *et al.*[7] reported a one-dimensional model of bubble growth and liquid flow and discussed the liquid ejection of the volume of up to $\sim 3 \times 10^5$ μm^3. After that, there was a history of development competition in the direction of making droplets smaller[19,20] in order to improve the image quality of inkjet printing; e.g., Bae *et al.*[16] proposed an inkjet head composed of two rectangular heaters and reported the liquid ejection of a volume of 30.9 pl with a velocity of 12 m/s. Sohrabi and Liu[17] reported a model of thermal inkjet and cell printing process using lattice Boltzmann methods. Khorram and Mortazavi[18] reported a direct numerical simulation on a horizontal surface in three dimensions. However, to the best of our knowledge, a launching phenomenon of a solid object using the vaporization of the liquid and the liquid ejection of large volume (e.g., ∼100 mm^3) has not been explored yet.

Plasma spray using an electric discharge phenomenon also has attracted much attention due to its practicality. Here, plasma spray is a device that sprays plasma particles using an arc discharge phenomenon mainly with an electro-static precipitator[6,21] or with high-speed gas.[22] Unlike the inkjet technology that ejects liquids such as ink, the plasma spray ejects ionized molecules. For example, Karthikeyan *et al.*[21] reported plasma spray synthesis of nanomaterials. Zhirkov *et al.*[23] reported the generation of supersize macroparticles of up to 0.7 mm in diameter due to a vacuum arc discharge from a Mo-Cu cathode. Shigeta[6] reviewed theoretical models and numerical methods to simulate turbulent thermal plasma flow transporting nanopowder. However, to the best of our knowledge, almost no study on liquid ejection using electric discharge has been reported so far, although there are many studies on discharge phenomena in water.[24–26]

Electrical discharge phenomena are important in various areas such as sterilization,[24] water treatment,[25] cancer treatment, dental

treatment,[22] atomic emission spectroscopy,[26] and plasma spray,[6,21] and thus, it has long been studied. For example, Zeleny[27] studied the electrical discharge in the air from liquid points and reported oscillation and falling-drop phenomena due to the electric force at the surface during intermittent discharge. Sano *et al.*[28] reported that nanoparticles are obtained in the form of floating powder on the water surface following an arc discharge between two-graphite electrodes in water. Zuev *et al.*[26] reported atomic emission spectroscopy using a boiling phenomenon due to electric discharges in test solutions, while Nicol *et al.*[22] reported the efficiency of low-temperature plasma treatments against bacteria using an atmospheric-pressure plasma jet. Furthermore, Starikovskiy *et al.*[29] reviewed non-equilibrium plasma in liquid water and discussed the dynamics of generation and quenching. However, no report has been made on a phenomenon in which a water droplet is launched upward from the surface of water due to electrical discharge in water.

Inkjet technology is important not only as a 2D graphical printing technology[5,19,20,30] but also as an additive manufacturing technology that includes 3D printing, bioprinting, maskless metal wiring, and non-contact liquid deposition technologies.[4,31–33] Thus, various inkjet technologies have been studied extensively. For example, Guan *et al.*[34] reported the internal flow behaviors during the Taylor cone formation of electrohydrodynamic (EHD) jet printing, while Sukhotskiy *et al.*[33] reported a computational study on printability regimes of molten metals for a magnetohydrodynamic (MHD) actuation. Gao *et al.*[31] reported the stable formation of a single metal droplet by a pneumatic actuator, while Kang *et al.*[35] reported the analysis of inkjet performance for a piezoelectric inkjet printhead of diameter 70 μm. However, to the best of our knowledge, techniques for launching solids, such as unmelted metals, have not been explored so far.

Overall, a launcher of a solid object using explosive vaporization due to electrical discharge in water has not been explored yet. Thus, we propose a centimeter-scale object launcher using explosive vaporization due to electrical discharge in water and examined the performance. In particular, we demonstrate that by the electrical discharge in the trapezoid-shaped chamber (hereafter trapezoid chamber), a centimeter-scale L-shaped piece of paper with 0.92 mg mass can be launched with an initial velocity ∼4 m/s, while a centimeter-scale paper airplane with 29.6 mg mass can be launched with the maximum velocity ∼2 m/s along a glass slide runway. In addition, to clarify the mechanism of solid launching phenomena, we systematically carried out vertical launching experiments of the centimeter-scale solid object of 60–340 mg. Moreover, as a central design concept peculiar to the solid launching device, we demonstrate the importance of water-repellent treatment of the solid surface.

II. EXPERIMENTAL METHODS

Figure 1 shows the schematic view of the centimeter-scale solid object launcher using explosive boiling with an electrical discharge. Specifically, Fig. 1(a) shows the plan view for a boiling experiment in a droplet. That is, we set a pair of Cu electrodes (enameled copper wires) of diameter $\phi_{Cu} = 1.0$ mm with a distance $D_1 = 2$ mm on a glass substrate coated with a water-repellent surfactant (water-repellent 1; Henkel Japan Co., LOCTITE: DBS-420), while we injected a distilled water droplet of 0.1 ml between the electrodes. Figures 1(b) and 1(c) show the photographs of the boiling phenomenon at $t = 0$ and 3/960 s, respectively, when we applied a DC pulse of high voltage V_0 (∼60 kV; catalog value) by a high-voltage pulse power supply (Walfront Co., ASIN: B07BFXNQ1S, arc ignition coil module). Here, for our measurement, the effective pulse width is ∼6 μs and the discharge (breakdown) current is ∼70 A. As shown in Fig. 1(c), we find that an explosive vaporization phenomenon occurs due to an electrical discharge phenomenon. Thus, our idea is to use this explosive vaporization to eject a liquid droplet from a chamber through a nozzle in one direction, and to use the force of the liquid to launch a solid object into the air.

Figures 1(d) and 1(e) show the plan and side views, respectively, for a launcher experiment using a trapezoid chamber. As shown in those figures, the trapezoid chamber (of internal volume 0.08 ml and height $H_2 = 5$ mm) was made of polyvinyl chloride (PVC) side walls of thickness 0.5 mm, a PVC rear wall of thickness 1 mm, a pair of Cu electrodes of diameter $\phi_{Cu} = 0.1$ mm with a distance $D_1 = 2$ mm, and the water-repellent glass substrate. Here, the Cu electrodes were placed at a height $H_3 = 1$–4 mm from the substrate, while an L-shaped piece of paper of length $L_2 = 4$ mm, height $H_4 = 3$ mm, depth 2 mm, and mass $m_p = 0.92$ mg was placed at the outlet as shown in Fig. 1(e). We tilted the substrate so that the elevation angle θ_1 was 3°, applied a high-voltage pulse of 60 kV, and observed the motion of the center gravity position (x_p, z_p) of the object with a video camera (Sony Co., Cyber-shot: DSC-RX100M4).

Figure 1(f) shows a side view for a launcher experiment using a U-shaped polyurethane tube chamber. The U-shaped chamber was made of a polyurethane tube of length $l = 35$ cm, inner diameter $D_2 = 5$ mm, and outer diameter $D_3 = 8$ mm. Here, a pair of Cu electrodes of diameter $\phi_{Cu} = 1.0$ mm with a distance $D_1 = 2$ mm were placed at a distance of $H_5 = 5$ mm from the right-side tube edge, while the right-side tube edge was directed vertically upwards; i.e., $\theta_1 = 90°$. By applying a high-voltage pulse of 60 kV, we observed the motion of the center gravity position (x_p, z_p) of the PVC square object ($L_5 \times L_5 = 10 \times 10$ mm^2) with a video camera. Note that the tube length above the electrodes is 0.5 cm, while the tube length behind the electrodes is 34.5 cm. Thus, the fluid mass in the lower part is 69 times larger than the mass of the fluid in the upper part. Consequently, the fluid in the lower part hardly moves against the sudden vaporization phenomenon between the electrodes, and thus droplets (of $\sim\pi 0.5 \times 0.25^2$ ml) are ejected upward.

Moreover, by analyzing the video data (of size 1920×1080 and frame rate 960 or 30 fps), we determined the position $\boldsymbol{x}_p = (x_p(t), z_p(t))$ of the flying object at a time t. From the data of $\boldsymbol{x}_p$, we obtained the velocity U_p as $U_p(t) \equiv \sqrt{\dot{x}_p(t)^2 + \dot{z}_p(t)^2} \simeq \sqrt{\left(\frac{x_p(t+\Delta t) - x_p(t)}{\Delta t}\right)^2 + \left(\frac{z_p(t+\Delta t) - z_p(t)}{\Delta t}\right)^2}$, where Δt (typically, 1/960, 3/960, or 1/30 s) is a time interval of the measurement. In particular, we define the initial velocity $U_{p,0}$ as $U_{p,0} \equiv U_p(0)$, while we determined the elevation angle θ_2 as $\theta_2 \equiv \tan^{-1}\frac{z_p(t+\Delta t)}{x_p(t+\Delta t)}$ at $t = 0$ s. Similarly, for a liquid ejection experiment without the solid object, we obtained the liquid edge position $\boldsymbol{x}_l = [x_l(t), z_l(t)]$ [Fig. 1(h)], the initial elevation angle θ_2' of the liquid edge, and the initial liquid velocity $U_{l,0}$. Note that we repeated the experiment N_s (typically, $N_s = 3$) times and N (=1 to N_s) denotes a trial number. Furthermore, the solid objects used here were usually surface-coated with water-repellent 1 (Henkel Japan Co., LOCTITE: DBS-420). Furthermore, the bubble in Figs. 1(g) and 1(h) is exaggerated; in fact, we have not observed a large single bubble like that in this study.

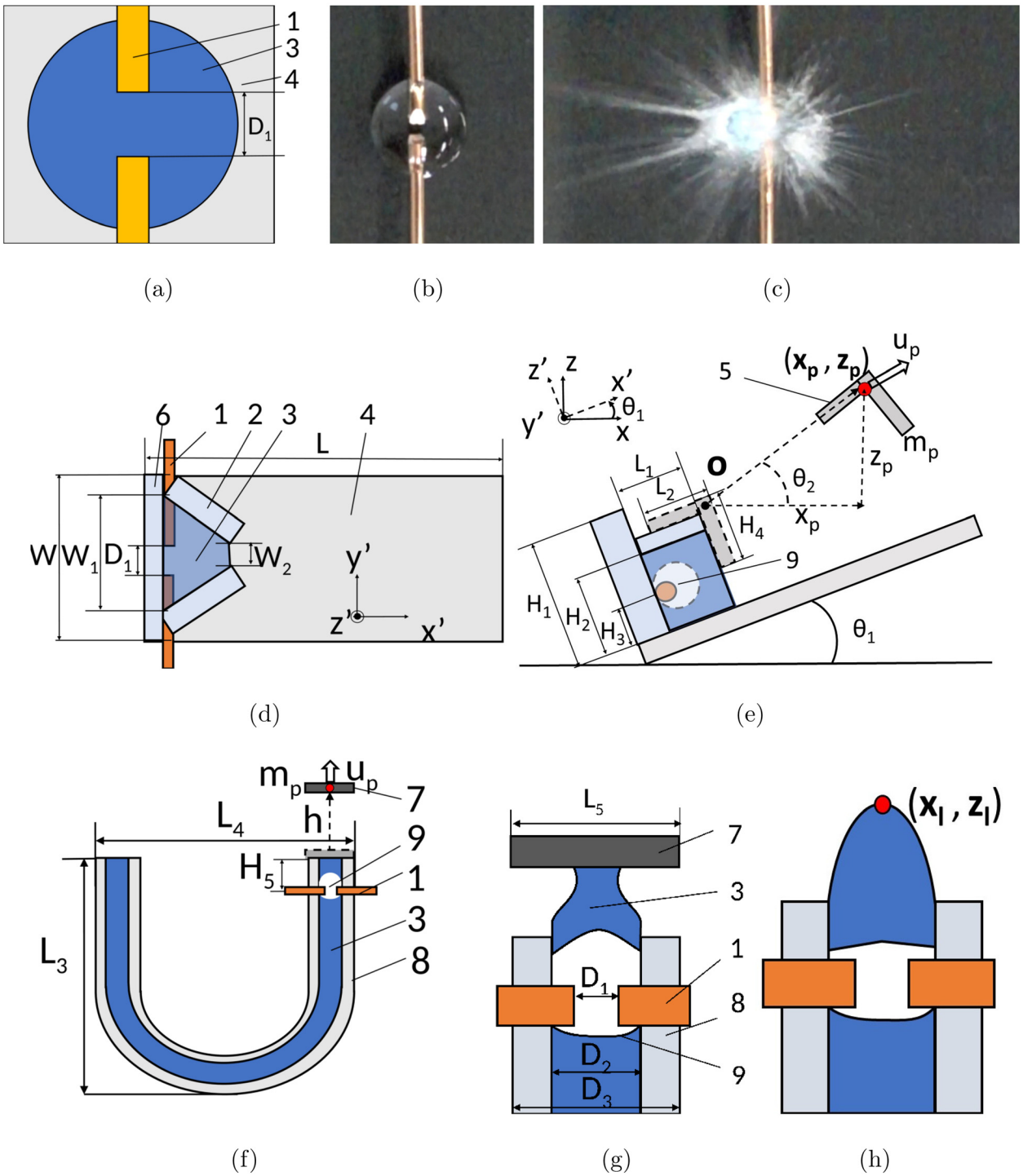

FIG. 1. Schematic view of the centimeter-scale solid object launcher using explosive boiling with discharge. (a) Plan view for a boiling experiment in a droplet. (b) and (c) Photograph of Expt. 1 at $t = 0$ and $t = 3/960$ s. (d) and (e) Plan and side views for a launcher experiment using a trapezoid chamber. (f) Side view for a launcher experiment using a U-shaped tube chamber. (g) Principle of the solid object launcher. (h) Edge of the liquid. 1: electrode, 2: sidewall of the chamber, 3: distilled water, 4: glass substrate, 5: L-shaped piece of paper, 6: rear wall of the chamber, 7: plastic (PVC: polyvinyl chloride) object, 8: polyurethane tube, 9: expanding water vapor (bubble). Here, $\theta_1 = 3^\circ$–90°, $m_p = 0.92$–340 mg. $W = 26$ mm, $W_1 = 8$ mm, $W_2 = 2$ mm, $L = 76$ mm, $H_1 = 10$ mm, $H_2 = 5$ mm, $H_3 = 1$–4 mm, $H_4 = 3$ mm, $H_5 = 5$–15 mm, $L_1 = 4$ mm, $L_2 = 4$ mm, $L_3 = 120$ mm, $L_4 = 170$ mm, $L_5 = 10$ mm, $D_1 = 2$ mm, $D_2 = 5$ mm, and $D_3 = 8$ mm.

III. RESULTS

In this result section, we will first demonstrate three typical launching phenomena in the diagonally upward direction using the electric discharge in a trapezoid-shaped chamber to clarify our proposed centimeter-scale solid and large-volume liquid launch technologies. That is, we will demonstrate the launching phenomenon of a centimeter-scale L-shaped piece of paper in Sec. III A, the high-speed ejection phenomenon of a large volume of water of the order of 100 mm^3 in Sec. III B, and the launching phenomenon of a centimeter-scale paper airplane in Sec. III C. Then, to clarify the mechanism of solid launching phenomena, we will present the results of systematically carried-out vertical launching experiments using a U-shaped chamber. That is, we will present the vertical launching phenomenon of the PVC plate in Sec. III D, the vertical liquid ejection phenomenon in Sec. III E, and the m_p and H_5 dependence in Sec. III F.

A. Launching of the L-shaped paper using a trapezoid chamber with electrical discharge

Figures 2(a)–2(c) show the photographs of the motion of the L-shaped solid object at $t = 5/960$, 9/960, and 13/960 s, respectively, under the condition that $H_3 = 2.5$ mm and $N = 1$. Here, the yellow dotted circles show the chamber position, the white broken arrows show the flying object, and the blue broken arrows show the edge of the liquid, which moves along the surface of the glass substrate.

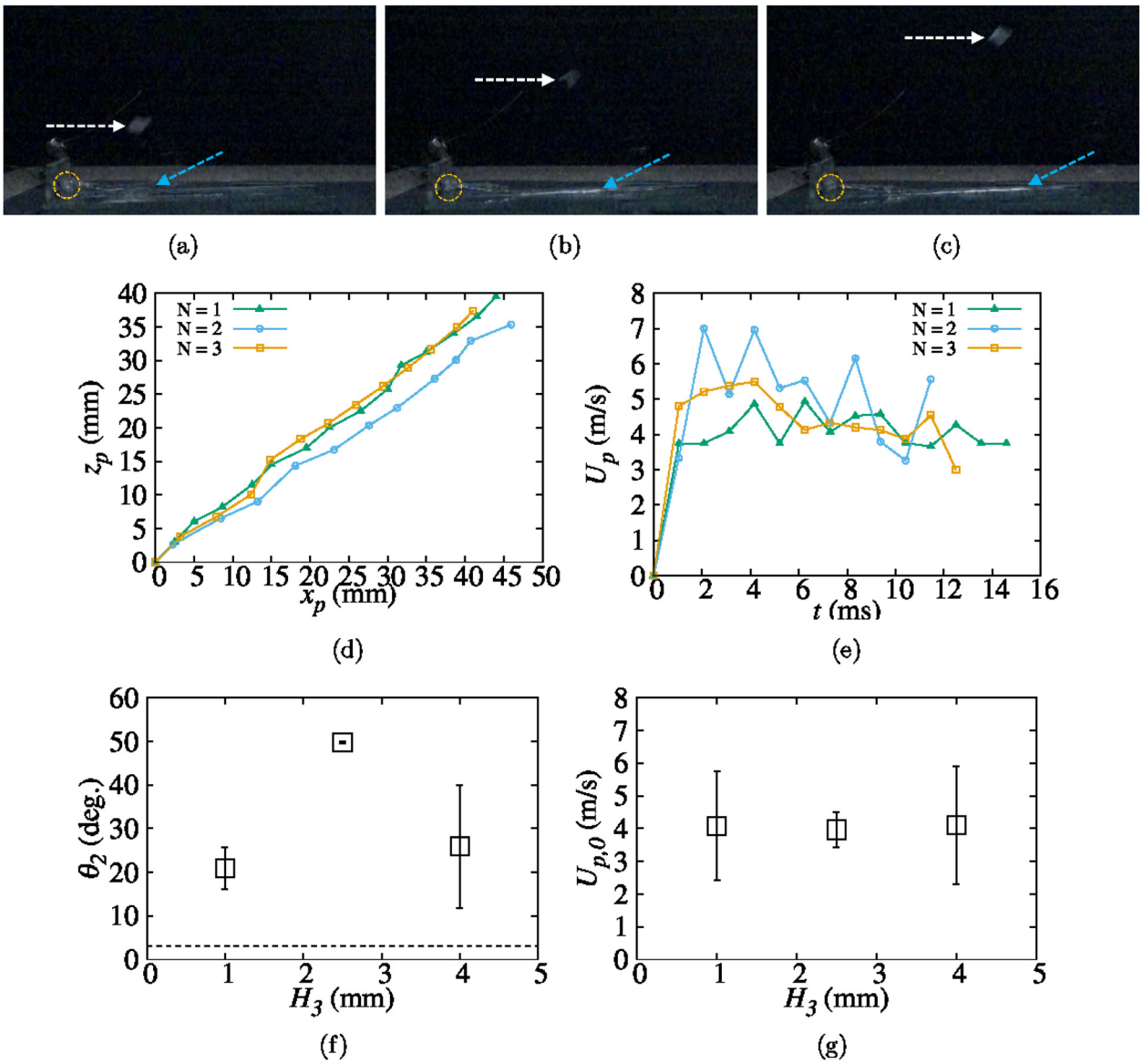

FIG. 2. Results of a solid launcher using a trapezoid chamber with an L-shaped object. (a)–(c) are the photographs at $t = 5/960$, 9/960, and 13/960 s, respectively, at $H_3 = 2.5$ mm and $N = 1$. (d) Trajectory of the object at $H_3 = 2.5$ mm. (e) U_p vs t at $H_3 = 2.5$ mm. (f) θ_2 vs H_3. (g) $U_{p,0}$ on H_3. Here, $m_p = 0.92$ mg and $\theta_1 = 3^\circ$.

Furthermore, Fig. 2(d) shows the trajectory of the L-shaped object, while Fig. 2(e) shows the dependence of U_p on t at $N = 1$–3 at $H_3 = 2.5$ mm. As shown in these figures, we found that by the electrical discharge in the trapezoid chamber, the L-shaped piece of paper with 0.92 mg mass was launched with an initial velocity ∼4 m/s [Fig. 2(e)] in the direction of an elevation angle $\theta_2 \simeq 50^\circ$ [Fig. 2(d)]. Furthermore, Figs. 2(f) and 2(g) show the dependence of θ_2 and $U_{p,0}$ on H_3, respectively. From these figures, we found that θ_2 became the maximum value (∼50°) at $H_3 = 2.5$ mm, while $U_{p,0}$ was approximately constant regardless of H_3. Here, the droplet hits the arm of the L-shaped piece of paper and changes its direction diagonally downward to the right. Therefore, the L-shaped piece of paper flies diagonally upward to the right while rotating.

B. Liquid ejection using a trapezoid chamber with electrical discharge

Figures 3(a)–3(d) show the photographs of the liquid ejection (without using a solid object) at $t = 2/960$, 3/960, 4/960, and 10/960 s, respectively, under the condition that $H_3 = 2.5$ mm and $N = 1$. From these figures, we found that water was ejected in a line, and eventually split into droplets [rectangular area in Fig. 3(d)] presumably because of surface tension. Furthermore, Fig. 3(e) shows the trajectory of the liquid edge, while Fig. 3(f) shows the dependence of U_l on t at $N = 1$–4 at $H_3 = 2.5$ mm. As shown in these figures, we found that by the electrical discharge in the trapezoid chamber, the liquid of ∼0.08 ml was ejected with an initial velocity of approximately 25–37 m/s [Fig. 3(f)] with a low elevation angle $\theta_2' \simeq 4^\circ$ [Figs. 3(e) and 3(g)]. Furthermore, Figs. 3(g) and 3(h) show the dependence of θ_2' and $U_{p,0}$ on H_3, respectively. From these figures, we found that θ_2' and $U_{l,0}$ became the minimum and maximum values ($\theta_2' \sim 4^\circ$ and $U_{l,0} \sim 28$ m/s), respectively, at $H_3 = 2.5$ mm. Since the gas phase due to rapid vaporization is generated linearly at the electrode and expands, droplets tend to be ejected diagonally upward to the right, rightward, and diagonally downward at $H_3 = 1.0$, 2.5, and 4.0, respectively. However, because of the rebound due to the substrate, θ_2' became positive values (∼6°) even at $H_3 = 4.0$ mm in Fig. 3(g).

C. Launching of the paper airplane using a trapezoid chamber with electrical discharge

Figures 4(a)–4(d) show the motion of the paper airplane of 29.6 mg mass for the trapezoid chamber at $t = 0/960$, 15/960, 30/960, and 45/860 s, respectively, at $\theta_1 = 45^\circ$ and $N = 1$. Here, we set the airplane at a pair of U-shaped guides near the nozzle for directional control and reduction of static friction, while the length, width, and height of the airplane are 20, 20, and 5 mm, respectively. Furthermore, Fig. 4(e) shows the trajectory of the airplane, while Fig. 4(f) shows the dependence of U_p on t at $N = 1$–3. In Fig. 4(e), the broken line shows the substrate of the runway. From these figures, we found that by the electrical discharge in the trapezoid chamber, the paper airplane with 29.6 mg mass was launched with the maximum velocity ∼1–2 m/s [Fig. 4(f)] approximately along a glass slide runway. Here, the maximum reachable altitude $z_{p,m}$ are ∼60–90 mm, while the maximum reachable distance $x_{p,m}$ are ∼200–300 mm. If we consider the theory of mass point motion ignoring air resistance, we obtain $z_{p,m} = \frac{(U_{p,0}\sin\theta_1)^2}{2g} \simeq 102$ mm and $x_{p,m} = \frac{U_{p,0}^2}{g}\sin 2\theta_1 \simeq 408$ mm for the condition that $\theta_1 = 45^\circ$ and $U_{p,0} = 2$ m/s. Thus, we found that the paper airplane did not glide farther than the expected distance (408 mm) of the analogous mass point. This is probably because we have not yet designed a way to push the airplane well. Therefore, we would like to solve the problem in the future.

D. Launching of the PVC plate using a U-shaped tube chamber with electrical discharge

Figure 5(a) shows the typical motion of the PVC plate of 60 mg for the U-shaped tube chamber at $N = 2$. Furthermore, Figs. 5(b) and 5(c) show the dependence of z_p and U_p on t, respectively, at $N = 1$–3. From these figures, we found that the PVC plate of 60 mg was launched to the maximum altitude $z_{p,m} \sim 15$–120 mm with an initial velocity $U_{p,0} \sim 0.3$–1.5 m/s while rotating. Figure 5(d) shows the dependence of $U_{p,0}$ and $z_{p,m}$ on m_p, while Fig. 5(e) shows the dependence of the maximum potential energy $E_z = m_p g z_{p,m}$ and the initial kinetic energy $E_k = \frac{1}{2} m_p U_{p,0}^2$ on m_p, respectively. In Fig. 5(d), the broken line shows the theoretical $U_{p,0}$ predicted from $\bar{E}_k$ ($U_{p,0}' = \sqrt{\frac{2\bar{E}_k}{m_p}}$), and the dotted line shows the theoretical $z_{p,m}$ ($= z_{p,m}'$) predicted from $\bar{E}_z$ ($z_{p,m}' = \frac{\bar{E}_z}{m_p g}$). As shown in Fig. 5(d), we find that $U_{p,0}$ and $z_{p,m}$ decrease as m_p increases. Furthermore, in Fig. 5(e), the broken line shows the average value of E_k ($\bar{E}_k \simeq 31.0$ μJ), while the dotted line shows the average value of E_z ($\bar{E}_z \simeq 46.2$ μJ). Here, although the average potential energy 46.2 μJ is larger than the initial kinetic energy 31 μJ, we consider that this is due to the large error bars because the average potential energy should decrease rather than increase relative to the initial kinetic energy due to the pullback effect of the surface tension of water (see Sec. IV C in detail) and the energy loss due to air resistance. Furthermore, although we expected physically that E_z and E_k would be constant, we find that there is a large fluctuation experimentally in E_k and E_z. Thus, to pursue a good application, we need to control this kind of fluctuation in the future.

E. Liquid ejection using a U-shaped tube chamber with electrical discharge

Figure 6(a) shows the photographs of the liquid ejection using a U-shaped tube chamber at $t = 0/960$, 10/960, 20/960, and 30/960 s under the condition that $m_p = 0$ mg (i.e., no solid present), $H_5 = 5$ mm, and $N = 1$. From these figures, we found that similar to the results of Fig. 3, water was ejected in a line, and eventually split into droplets because of surface tension. Furthermore, Figs. 6(b) and 6(c) show the dependence of U_l and z_l on t, respectively, at $N = 1$–3. From those figures, we obtained that the initial velocity of water (of ∼0.10 g) is 5.909 ± 0.881 m/s, while the initial kinetic energy $E_{k,l}$ of water is 1.714 mJ. Thus, the utilization efficiency $\eta_{z,a} \equiv \frac{\bar{E}_z}{E_{k,l}}$ is ∼2.7%. Therefore, we may need to increase $\eta_{z,a}$ in the future.

F. Dependence of $U_{p,0}$, $z_{p,m}$, E_k, and E_z on m_p and H_5 for the U-shaped tube experiment

Figures 7(a)–7(d) show the dependence of $U_{p,0}$, $z_{p,m}$, E_k, and E_z on m_p, respectively, at $H_5 = 5$–15 mm for the U-shaped tube experiment. Here, since we performed the same experiment again, the data at H_5 are different from the data in Fig. 5. Furthermore, the large difference in $z_{p,m}$ at $m_p = 60$ mg is due to the difference in the number of

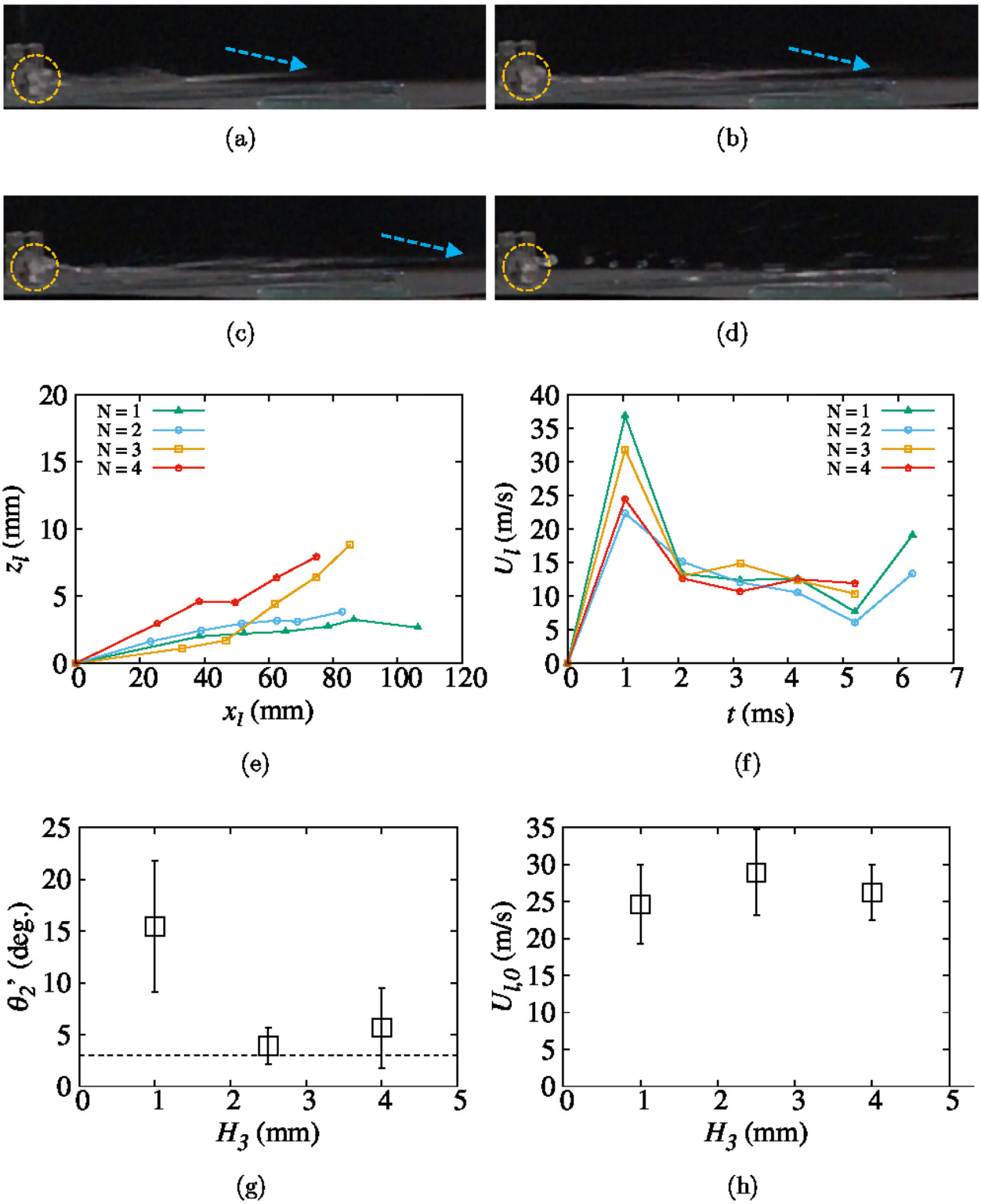

FIG. 3. Results for a liquid ejection using a trapezoid chamber. (a)–(d) are the photographs at $t = 2/960$, 3/960, 4/960, and 10/960 s, respectively, at $H_3 = 2.5$ mm and $N = 1$. (e) Trajectory of the liquid edge (x_l, z_l) at $H_3 = 2.5$ mm. (f) U_l vs t at $H_3 = 2.5$ mm. (g) θ_2' vs H_3. (h) $U_{l,0}$ vs H_3. Here, $\theta_1 = 3°$.

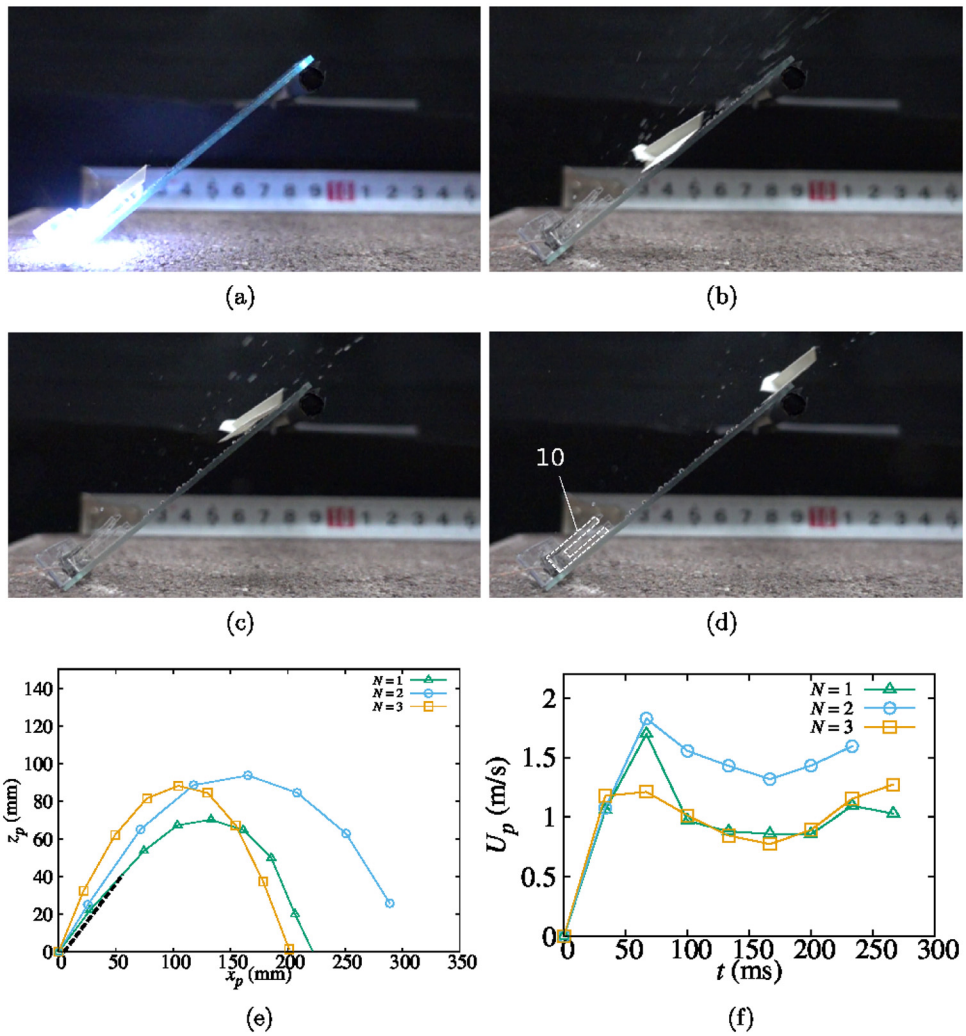

FIG. 4. Airplane launching using a trapezoid chamber. (a)–(d) show the motion of the paper airplane for the trapezoid chamber at $t = 0/960$, 15/960, 30/960, and 45/860 s, respectively, at $N = 1$. (e) z_p vs x_p. (f) U_p vs t. 10: U-shaped guide. Here, $m_p = 29.6$ mg and $\theta_1 = 45°$.

the event when flying high, as will be discussed later. From those figures, we find that there is a tendency that $U_{p,0}$ and $z_{p,m}$ decrease as m_p increase, while there is a tendency that $U_{p,0}$ and $z_{p,m}$ have the maximum at $m_p \sim 200$ mg.

Figures 8(a)–8(d) show the dependence of $U_{p,0}$, $z_{p,m}$, E_k, and E_z on H_5, respectively, at $m_p = 60$ to for the U-shaped tube experiment. From those figures, we find that there is a tendency that $U_{p,0}$, $z_{p,m}$, E_k, and E_z decrease as H_5 increases. Furthermore, in Figs. 8(c) and 8(d), E_k and E_z seem to have similar values to each other. Thus, we can neglect the rotational energy as the first step.

Figures 9(a) and 9(b) show the dependence of $U_{l,0}$ and E_k on H_5 (at $m_p = 0$ mg) for the liquid ejection experiment using a U-shaped chamber. From those figures, we find that there is a tendency that $U_{l,0}$ and E_k decrease as H_5 increases. Furthermore, Fig. 9(c) shows the dependence of the energy efficiency $\eta_z \left(\equiv \frac{E_z}{E_{k,l}}\right)$ on m_p at $H_5 = 5$–15 mm, while Fig. 9(d) shows the dependence of the energy efficiency $\eta_{z,a} \left(\equiv \frac{\bar{E}_z}{E_{k,l}}\right)$ on H_5. Here, $\eta_{z,a}$ involves averaging over different object masses, while η_z is the efficiency for each object. From Fig. 9(c), we find that there is a tendency that η_z has the maximum value at $m_p = 200$ mg. Furthermore, we find that the values of η_z at $H_5 = 5$ mm seem to be much smaller than the values at $H_5 = 10$ and 15 mm. Moreover, from Fig. 9(d), we find that there is a tendency that $\eta_{z,a}$ increases as H_5 increases. Note that in Fig. 9, the data for $H_5 = 5$ mm are taken separately from the experiment in Figs. 5 and 6 by using a similarly made different device. Thus, $\eta_{z,a}$ (∼4.5%) at $H_5 = 5$ mm in Fig. 9(d) is much higher than the value (∼2.7%) obtained from the experiment in Figs. 5 and 6 due to the fluctuation of the experimental data.

IV. DISCUSSION

This discussion section is presented in Subsections IV A–IV F. For a better understanding of phenomena near the electrodes caused by underwater discharge, we will discuss the additional experimental

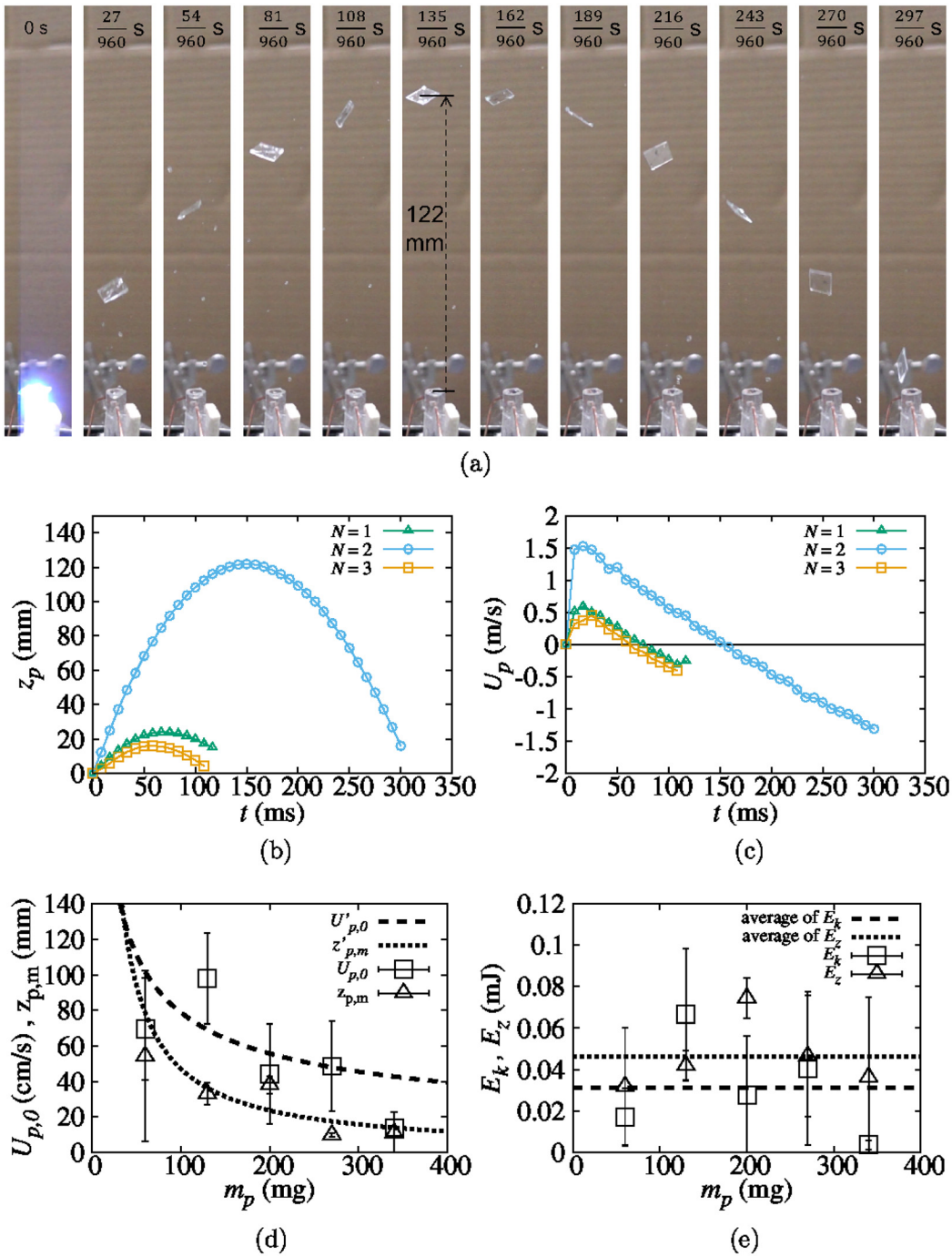

FIG. 5. PVC plate launching using a U-shaped tube chamber. (a) Photographs of the PVC object of $m_p = 60$ mg at $N = 2$. (b) z_p vs t at $m_p = 60$ mg. (c) U_p vs t at $m_p = 60$ mg. (d) $U_{p,0}$, $z_{p,m}$ vs m_p. (e) $E_k = \frac{1}{2} m_p U_{p,0}^2$, $E_z = m_p g z_{p,m}$ vs m_p.

results of the fine bubbles near the electrode and the state of the water surface in Sec. IV A and for the electrical input energy in Sec. IV B. Furthermore, to clarify the central design concept peculiar to the solid launching device, we will discuss the additional experimental results for the effect of the surface tension in Sec. IV C and for the deformation of the solid object due to the impact of the water pressure in Sec. IV D. Then, after discussing the effects of geometry and fluid friction, we will finally discuss the significance of this manuscript.

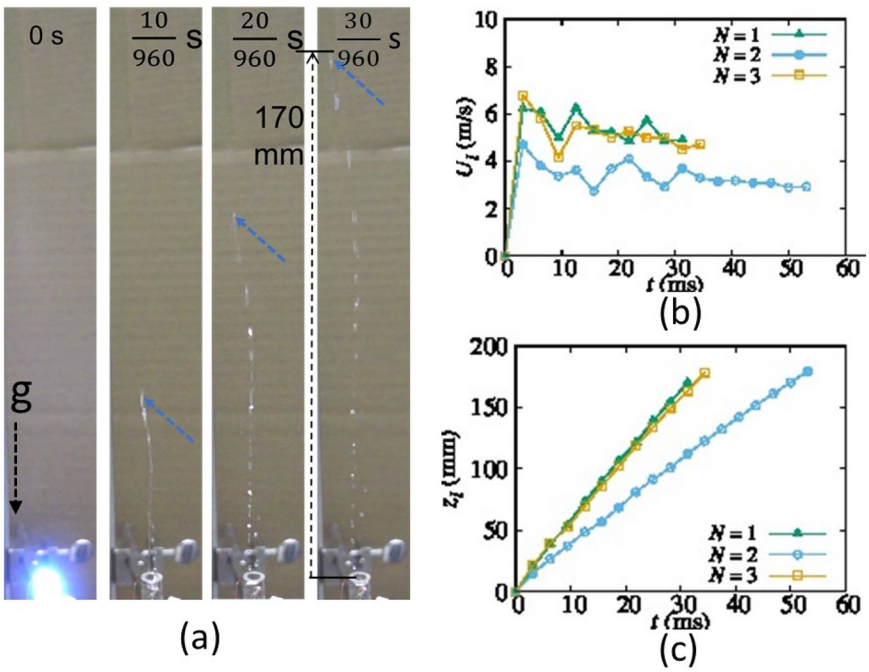

FIG. 6. Liquid ejection using a U-shaped tube chamber without a solid object. (a) Photographs of the ejected liquid motion at $m_p = 0$ mg (i.e., no solid present) at $N = 1$. (b) U_l vs t. (c) z_l vs t. In (a), the arrows show the edge of the ejected liquid.

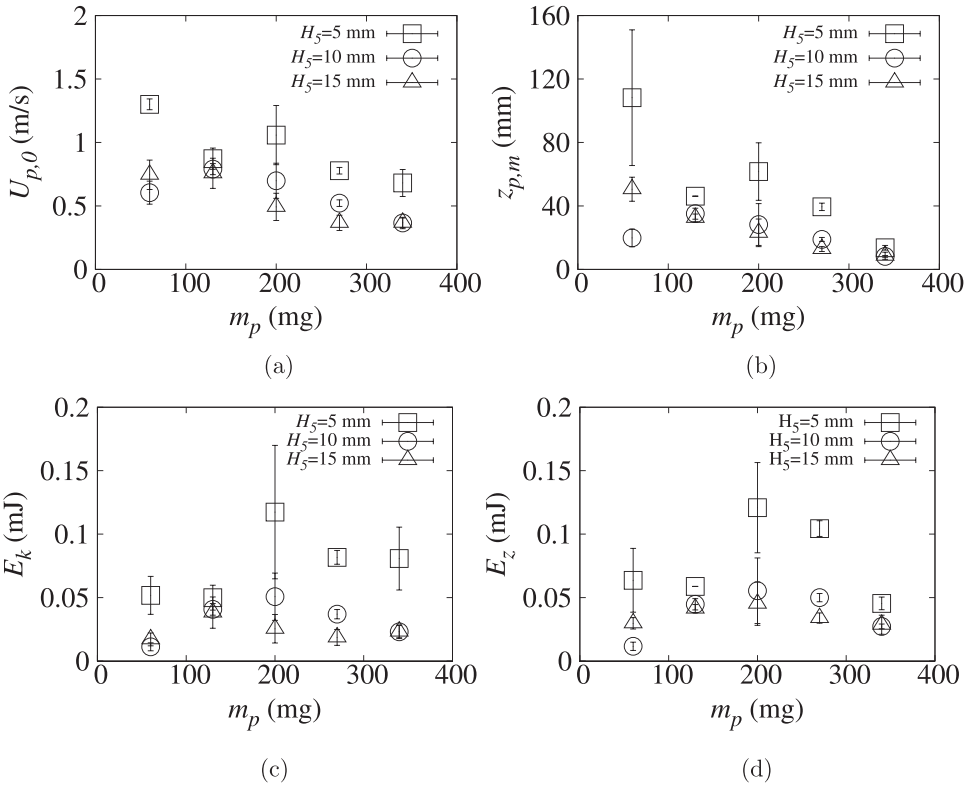

FIG. 7. Dependence of $U_{p,0}$, $z_{p,m}$, E_k, and E_z on m_p at $H_5 = 5$–15 mm for the U-shaped tube experiment (solid launching experiment). (a) $U_{p,0}$ vs m_p. (b) $z_{p,m}$ vs m_p. (c) E_k vs m_p. (d) E_z vs m_p.

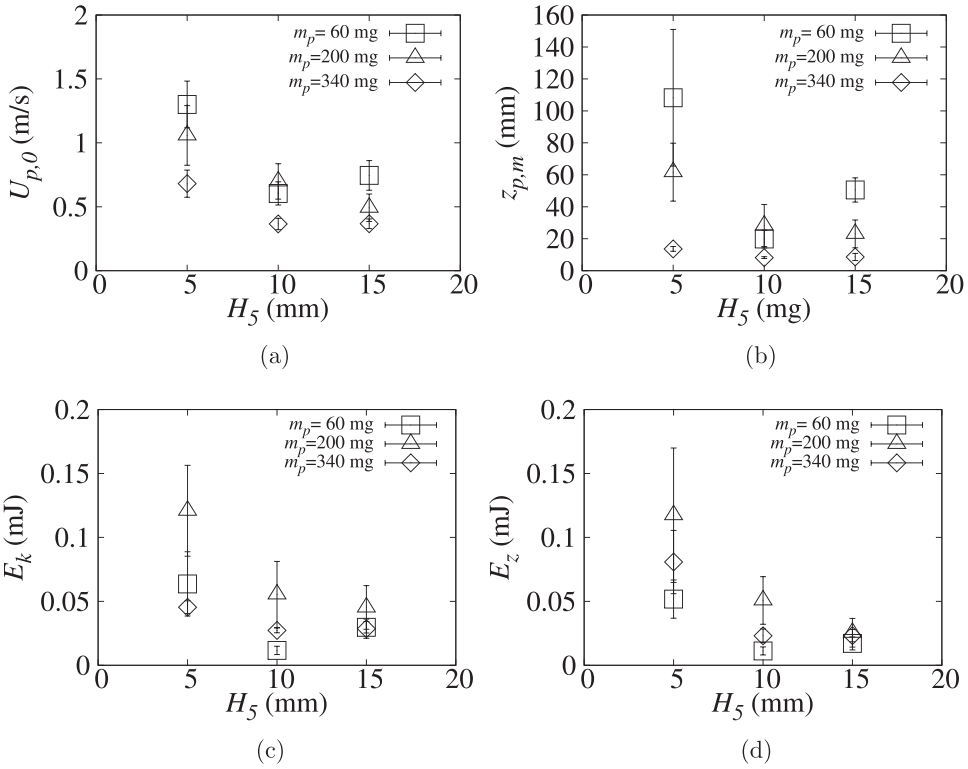

FIG. 8. Dependence of $U_{p,0}$, $z_{p,m}$, E_k, and E_z on H_5 at $m_p = 60$–340 mg for the U-shaped tube experiment (solid launching experiment). (a) $U_{p,0}$ vs H_5. (b) $z_{p,m}$ vs H_5. (c) E_k vs H_5. (d) E_z vs H_5.

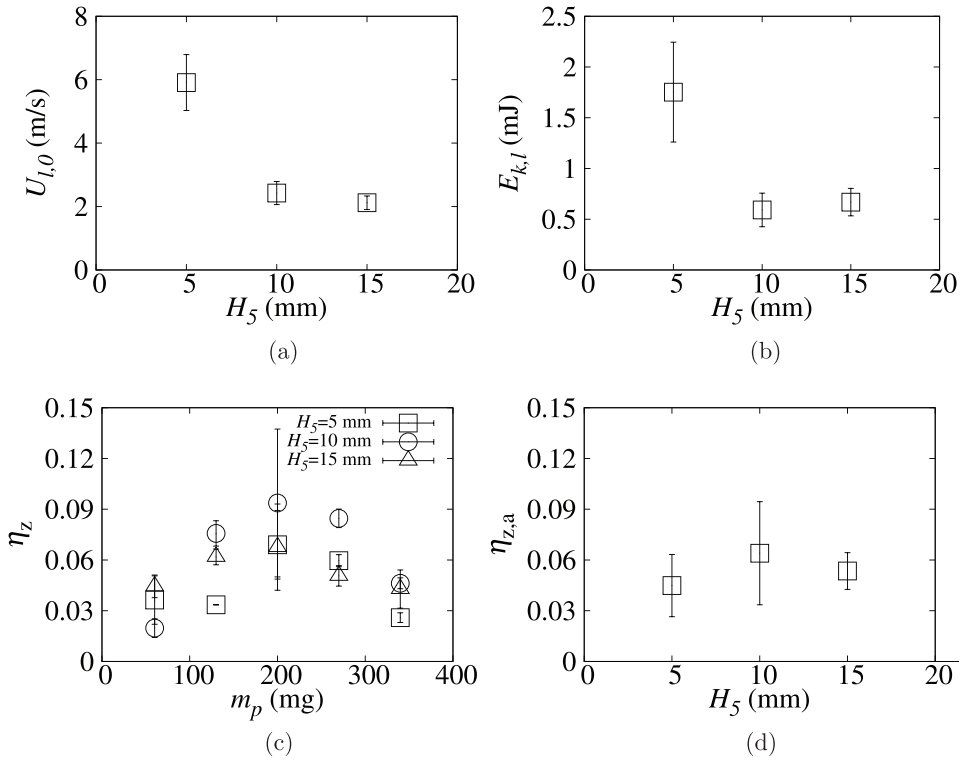

FIG. 9. Dependence of $U_{l,0}$, E_k, η_z, and $\eta_{z,a}$ on H_5 (at $m_p = 0$ mg) for the liquid ejection experiment using a U-shaped tube chamber (liquid launching experiment and the efficiency of the solid launching). To obtain $E_{k,l}$, we assume that the liquid in the region above H_5 is ejected, although it is corrected in Fig. 15. (a) $U_{l,0}$ vs H_5. (b) $E_{k,l}$ vs H_5. (c) η_z vs m_p. (d) $\eta_{z,a}$ vs H_5.

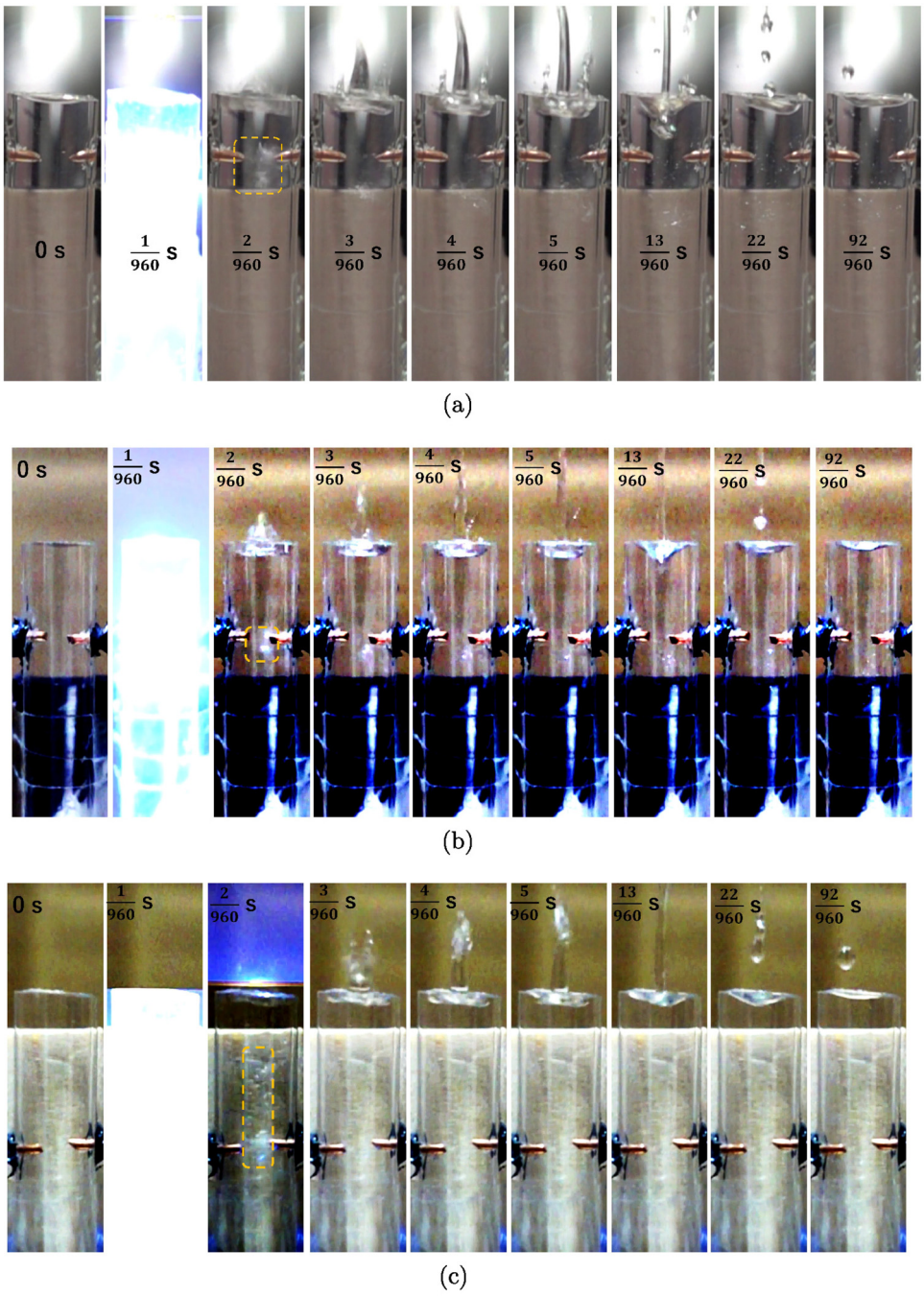

FIG. 10. Generation of fine bubbles near the electrode and state of the water surface for the liquid ejection experiment using a U-shaped tube chamber. Here, the area bounded by the broken lines shows remnants of fine bubbles.

A. About the additional experiment for the generation of fine bubbles near the electrode and state of the water surface

Figure 10 shows the typical results of the additional experiment for the generation of fine bubbles near the electrode and the state of the water surface for the liquid ejection experiment using a U-shaped tube chamber at $H_5 = 5$–15 mm. Here, although Fig. 10(a) is a raw image, Figs. 10(b) and 10(c) show contrast-enhanced images. In Figs. 10(a)–10(c), the first image shows the initial state before applying the high voltage between the electrodes, while the second image shows

the image during the electrical discharge. By comparing the first image with the third image, we can recognize that a white cloud exists in the third image; i.e., we consider that the area bounded by the broken lines shows remnants of fine bubbles. In other words, unlike ordinary liquid ejection,[7] no bubble expansion was observed. Furthermore, from Figs. 10(a)–10(c), we found that only the center part of width ∼1–2 mm (of a water surface) protruded and eventually ejected, while the water level of the surrounding part became lower to compensate the water loss due to the liquid ejection. Note that the generation of the single bubble due to rapid heating is well-known as a film boiling,[7] while a single bubble due to the underwater spark was reported by several authors[36–39] in a large chamber. In particular, Vokurka and Plocek[38] reported a large bubble accompanying fine bubbles. Thus, we interpreted that mainly a single bubble grows and disappears within 1 ms, and fine bubbles are observed. Furthermore, we also interpret that the inertial effect due to the rapid expansion of a single bubble causes the solid to be ejected (as shown in Fig. 1), although we have not observed the single bubble yet.

From the above argument, we may need to correct our estimation of the ejected liquid mass. Figure 11(a) shows the schematic view of the measurement of H_6 and H_7, where H_6 shows the liquid level drop in a steady state, while H_7 shows the liquid level drop just after the liquid ejection. As shown in Fig. 11(a), since the right and left water surfaces try to reach the same level at the steady state, there is a relation that $H_7 = 2H_6$ and $m_l = \pi(\frac{D_2}{2})^2 H_7 \rho$, where ρ is the density of water. Here, we directly measured H_7 because an oscillation phenomenon was observed in the measurement of H_6. Figure 11(b) shows the dependence of H_7/H_5 on H_5. From Fig. 11(b), we find that only 70%, 20%, and 10% of the liquid above the electrodes were ejected at $H_5 = 5$, 10, and 15 mm, respectively. Figures 11(c) and 11(d) show the dependence of the corrected m_l and $E_{k,l}$, respectively. As shown in Fig. 11(c), we find that the ejection mass of liquid decreases rapidly with H_5. Furthermore, we find that our device can eject the liquid up to 70 mg. In other words, our device can launch heavier mass for the solid–liquid ejection mode than that for the only-liquid ejection mode. Thus, we consider that launching a solid object is a different process from first launching a liquid droplet and then transferring some of the droplet energy to a solid.

B. About the additional experiment for the electrical input energy

Figure 12 shows the results of the additional experiment for the electrical input energy. Typically, we observed two kinds of behaviors. The one is a mode (mode A) in which a discharge current ($V_{0,d} \sim 70$ V) flows for a moment (∼40 ns), and then, the current does not recover [Fig. 12(a)]. The other is a mode (mode B) in which a discharge current ($I_{0,d} \sim 60$ A) flows for a moment, and then, the current recovers [Fig. 12(b)]. Here, the solid object of $m_p = 130$ mg launched in the level of $z_{p,m} \sim 6$–7 cm for mode B, while it launched in the level of $z_{p,m} \sim 4$ cm for mode A. Thus, we consider that the reason for the large fluctuation is due to the difference of these modes for the current and voltage behavior of the discharge phenomenon. Furthermore, since the launching ability of modes A and B is in the same order, we consider that the effective discharge time t_d for the rapid boiling is ∼40 ns. Here, the 40 ns estimate comes from the

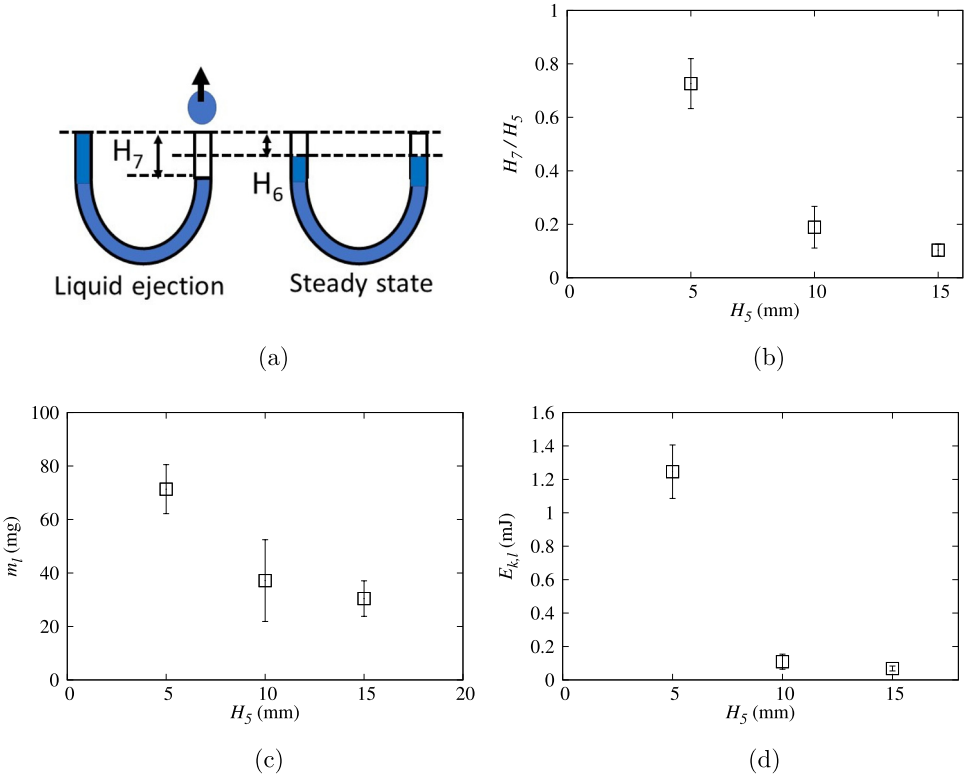

FIG. 11. Results of the measurement of the ejected liquid volume for the only-liquid ejection mode. (a) Measurement of the ejected liquid. (b) H_7/H_5 vs H_5. (c) m_l vs H_5. (d) Correction of Fig. 9(b). Here, $m_l \simeq \rho S_0 H_7$ is the liquid ejection mass.

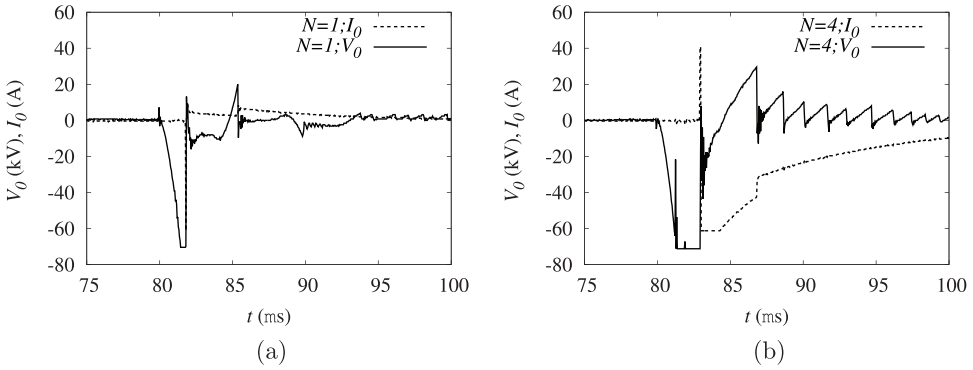

FIG. 12. Dependence of V_0 and I_0 on t. (a) I_0, V_0 vs t ($N = 1$, mode A). (b) I_0, V_0 vs t ($N = 4$, mode B). Here, $H_5 = 5$ mm and $m_p = 130$ mg.

duration time of a discharge current for mode A in Fig. 12(a). Note that in Fig. 12(a), the current characteristic of mode A (a broken line) is a pulse-like response with a short pulse width of ∼40 ns, which overlaps with the voltage characteristic (a solid line); thus, it is difficult to see in Fig. 12(a). Therefore, the electrical input energy E_e concerning to the rapid boiling can be estimated as $E_e \sim V_{0,d} I_{0,d} t_d \sim 168$ mJ. Since the observed maximum kinetic energy is ∼0.15 mJ at most [Fig. 8(c)], we understand that the only 0.1% of the input electrical energy can convert to the kinetic energy of the solid. Thus, we consider that there is a lot of room for the improvement of our device in the future. Note that the voltage oscillation seen after the discharge (in Fig. 12) is known as the ringing noise caused by the reflection of the signal at both ends of the wire. Furthermore, by considering the spark delay time (∼3 μs) and the width of the recovered current (∼3 μs), we estimate that the effective pulse width generated by the ignition coil is ∼6 μs for our experiment.

C. About the effect of the surface tension

The surface water-repellent treatment of a solid object plays an important role in the launching problem of the solid. Figure 13 shows the results of the additional experiment for the effect of the surface tension. Specifically, Fig. 13(a) shows the comparison of the maximum launching height $z_{p,m}$ with and without surface water-repellent treatment for five trials. Here, treatments 1 and 2 denote the surface water-repellent treatments using water-repellent 1 (Henkel Japan Co., LOCTITE: DBS-420) and 2 (CCI Co., smart view), respectively, while solid, dotted, and broken lines are the average values for no treatment, treatment 1, and treatment 2, respectively. From Fig. 13(a), we find that the average of $z_{p,m}$ for no treatment (102 mm; dotted line) is much lower than that for the repellent treatments (126 mm for water-repellent 1, 164 mm for water-repellent 2). In detail, in Fig. 13(a), triangles show the results when only bubbles entered into the tube without any solid launch occurring for the first voltage application [as shown in Fig. 13(b)]. Thus, we find that the launching phenomenon of the solid fails with a probability of 60% without water-repellent treatment, whereas the launching phenomenon occurs with a probability of 100% with water-repellent treatment. Furthermore, the cross with the triangle shows the launching ability for the second voltage application for the object without water-repellent treatment, after bubbles enter [as shown in Fig. 13(c)]. Therefore, we find that the solid object with no treatment also can be launched if bubbles enter between the solid and liquid. Moreover, from Fig. 13(c), we find that the droplets deform and splatter in the horizontal direction, similar to droplet collision, in the launching phenomenon of a solid with bubbles in the tube. Figures 13(d)–13(f) show the images of the launching phenomenon without bubbles immediately after launch (at $t = 1/960$ s) for the results corresponding to the no treatment, treatment 1, and treatment 2, respectively. From these figures, we find that the diameter of the water column ejected with water-repellent treatment is much smaller than that without water-repellent treatment. Therefore, from the above facts, we interpreted that on the one hand, the solid object without the water-repellent treatment suffers the strong force due to the surface tension of water in the downward direction if no bubble exists. On the other hand, the surface tension force weakens significantly if bubbles exist. In addition, it weakens significantly if the solid object is surface-coated with water-repellent.

D. About the deformation of the solid due to the impact of the water pressure (for no treatment)

Figure 14 shows the deformation of the solid surface due to the water pressure for no treatment when the solid was not launched by the first voltage application. In this case, although the solid surface was initially flat at $t \sim -1/960$ s [Fig. 14(a)], it deformed into a convex shape during discharge at $t \sim 0$ s [Fig. 14(b)]; then (at $t \sim +1/960$ s), it became a concave shape [Fig. 14(c)]. Here, we consider that this is due to the impact effect on the solid surface. Furthermore, from Fig. 14(c), we found that a bubble entered the chamber during the deformation process of the solid. Moreover, no significant deformation was observed when the solid was launched by the voltage application (for water-repellent 1 and 2). This is probably because the constraint by surface tension is weak.

E. About the effects of geometry and fluid friction (D_2 dependence)

To clarify the effects of geometry and fluid friction, we performed the additional experiment at $D_2 = H_5 = 4$ mm and $m_p = 60$ mg. Specifically, Figs. 15(a)–15(c) show the dependence of $Z_{p,m}$, H_7/H_5, and m_l on the tube-diameter D_2, respectively, under the condition that $H_5 = D_2$. As shown in Fig. 15(a), we find that $z_{p,m}$ is approximately constant at $4 \leq D_2 \leq 5$ mm; i.e., $U_{p,0} \simeq \sqrt{2gz_{p,m}}$ is also approximately constant. Here, since it is well known that the pressure loss due

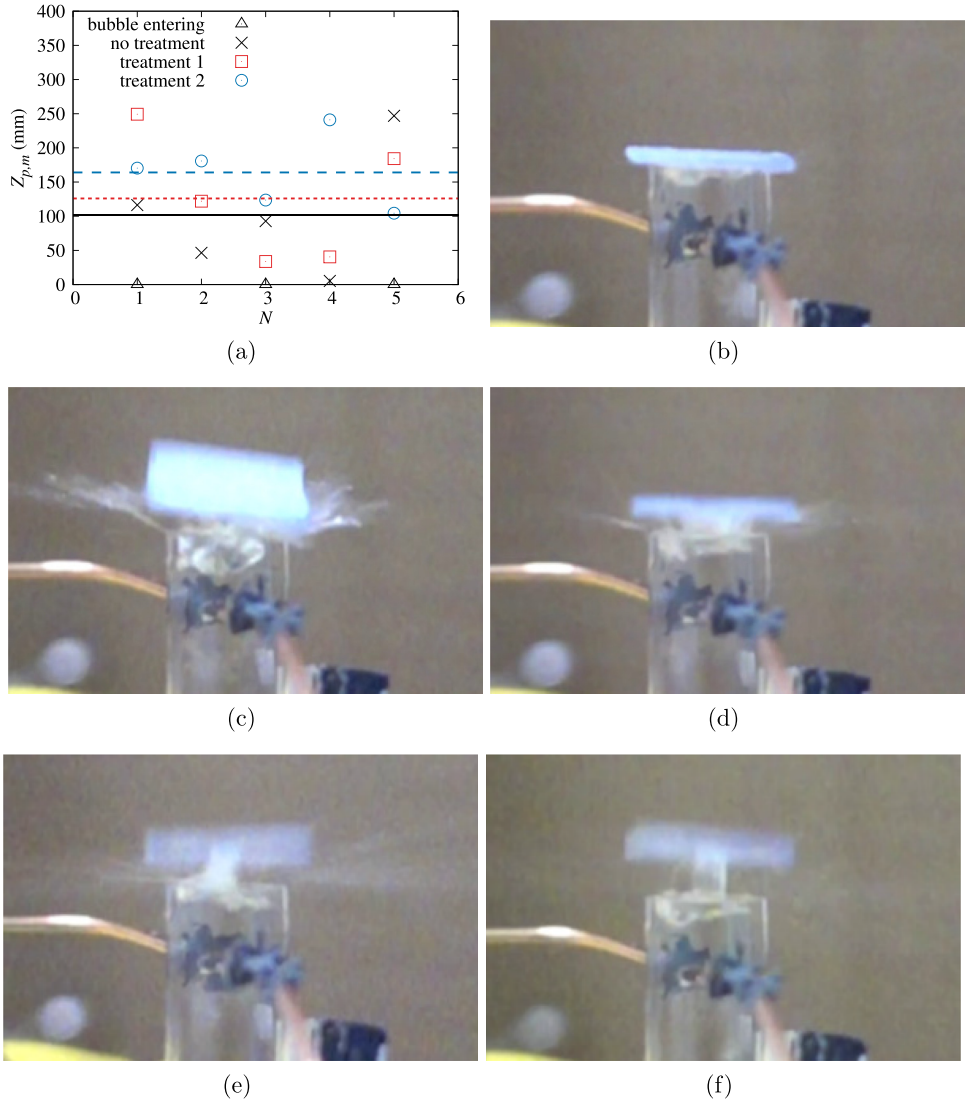

FIG. 13. Experimental results for the effect of the surface tension. In (a), treatments 1 and 2 denote the surface water-repellent treatments using water-repellent 1 (Henkel Japan Co., LOCTITE: DBS-420) and 2 (CCI Co., smart view), respectively, while solid, dotted, and broken lines are the average values for no treatment, treatment 1, and treatment 2, respectively. (a) Comparison between the treatments. (b) Bubble entering by a pulse (no treatment). (c) Launch by 2nd pulse (no treatment). (d) Launch by a pulse (no treatment). (e) Launch by a pulse (water-repellent 1). (e) Launch by a pulse (water-repellent 2). Here, $H_5 = 5$ mm and $m_p = 60$ mg; in (b) to (f), $N = 1$ and $t = 1/960$ s.

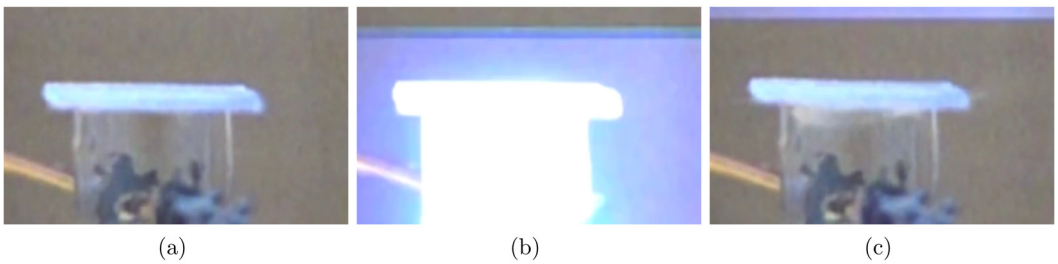

FIG. 14. Deformation of the solid surface due to the water pressure for no treatment. (a) Before deformation. (b) Convex deformation. (c) Concave deformation. Here, $N = 1$, $H_5 = 5$ mm, and $m_p = 60$ mg.

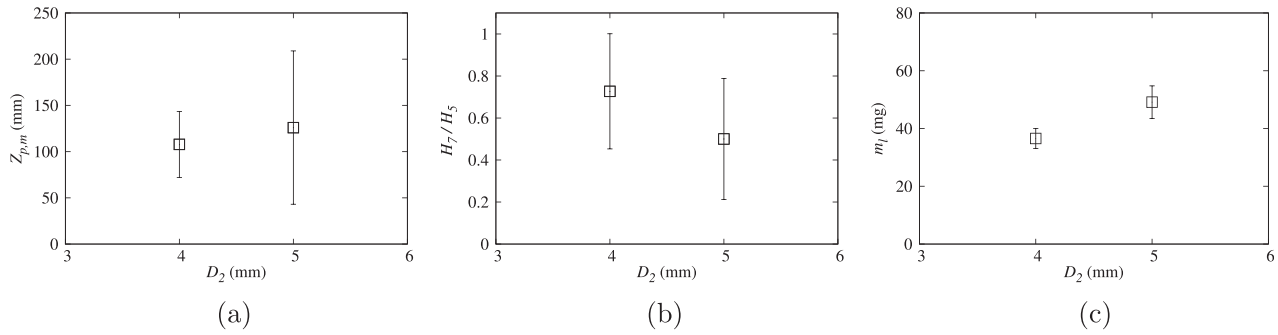

FIG. 15. Effect of the geometry and viscosity problems (D_2 dependence). (a) $z_{p,m}$ vs D_2 (water repellent). (b) H_7/H_5 vs D_2. (c) m_l vs D_2. Here, $N = 1$ and $m_p = 60$ mg.

to fluid friction ΔP_{loss} of the tube is proportional to $\sim \frac{\mu U_{p,0}^{7/4}}{D_2^{5/4}}$ (please see Blasius' formula with Darcy–Weisbach equation[40]), ΔP_{loss} increases 1.32 times when D_2 changes from 5 to 4 mm, where μ is the viscosity coefficient (the viscosity in the narrow sense) of water. Thus, we can interpret that the reason why the change in D_2 is small is that the influence of the fluid friction (viscous force or viscosity phenomenon in a broad sense) on $z_{p,m}$ is small. In other words, although Fig. 15 shows the D_2 dependence, it also shows the effects of geometry and fluid friction. Furthermore, from Figs. 15(b) and 15(c), we find that although H_7/H_5 decreases with D_2, m_l increases with D_2. Furthermore, we find that we can launch the solid object of 130 mg mass with liquid of up to 50 mg mass.

F. Significance of this manuscript

1. 10^6 times launching ability of mass than the previous work

Although micro-liquid ejector is widely used commercially, we have first explored the launching problem of a centimeter-scale solid object using an explosive vaporization phenomenon of liquid. In particular, we have first demonstrated that a centimeter-scale object can be launched by the water force ejected from a chamber (nozzle) due to the explosive boiling resulting from electrical discharge and succeeded in launching a centimeter-scale object of 0.92–340 mg in the vertical or oblique directions. In other words, our device can launch $\sim 10^6$ larger mass than the previous device (Asai *et al.*'s device[7]), which can launch the droplet of $\sim 3 \times 10^{-7}$ g. In addition, we succeeded in ejecting a large water droplet of $\sim 100\ \text{mm}^3$ (~ 0.1 g) with a high velocity of up to 30 m/s by the expansion of the water of gas phase resulting from electrical discharge, under the condition that there is no solid object; i.e., our device can eject $\sim 3 \times 10^5$ larger liquid than the previous device (Asai *et al.*'s device[7]), which can eject the droplet of $\sim 3 \times 10^{-4}\ \text{mm}^3$. Therefore, our device is innovative.

2. The first launching study using the explosive boiling due to electrical discharge

Here, the extremely high launching ability results from the use of explosive boiling due to electrical discharge in water. Although there are many studies on discharge phenomena in water,[24–26] we have first reported the large-mass launching phenomenon using the explosive boiling due to electrical discharge. In particular, as shown in Fig. 10, we have first reported that a water droplet can be launched upward from the surface of water due to electrical discharge in water; i.e., we found that when the diameter of the tube chamber is much larger than the electrode distance (i.e., $D_2 \gg D_1$), only the center part of the surface protruded and eventually ejected, while the water level of the surrounding part became lower to compensate for the water loss due to the liquid ejection.

3. The first launching technology for micro-aerial vehicles (MAVs) using a boiling phenomenon

Launching technologies for a centimeter-scale solid object are important ranging from seed ejection of plants[3] to micro-aerial vehicles (MAVs).[1,2] For example, Li *et al.*[3] demonstrated a bionic ejection device using bent sheet structures inspired by a seed ejection mechanism of plants, while Chen *et al.*[2] reported a hovering flight inspired by the flying of insects. However, the liftoff of MAVs is a challenging problem even now. Thus, in this manuscript, we have shown that our device can launch a paper airplane with a 29.6 mg mass from a launch pad. We consider that our launching technology can contribute to the liftoff problem of other MAVs in the future. Furthermore, it is usually difficult to throw an object without rotating it (as shown in Fig. 5). Thus, we have shown that even a rotating L-shaped object can be launched stably without showing a complicated rotating flight path, as a first step. In addition to that, we consider that the L-shaped solid object is practically important because it allows simple and stable installation on the inclined launch pad.

4. Clarification of the central design concept for solid launching devices

We have first clarified the importance of water-repellent treatment of the solid surface as a problem peculiar to solid launching devices using water ejection by the electric discharge. That is, we find that the launching phenomenon of the solid fails with a probability of 60% without water-repellent treatment, whereas the launching phenomenon occurs with a probability of 100% with water-repellent treatment. This fact can be interpreted as the water-repellent treatment weakens the pullback force due to the surface tension of water and enables the separation of water and solids; consequently, it enables our device to launch the solid object with a single discharge.

5. Applications of our device

Innovative crop or fruit protector from pests and birds:

As the world's population grows, producing enough food has become a critical issue. In particular, the transition from conventional pesticide-based crop protection to a more sustainable integrated pest management (IPM) framework is required.[41,42] Above all, the damage caused by birds in orchards is serious;[42] e.g., 0.84 cherries min^{-1} ha^{-1} were lost from orchards and the financial loss of $2.2 to $2.4 million is approximately occurring even in the state of Michigan over a 5-year period.[42] Here, our launcher can be made to launch water or small objects on demand in response to signals from the microcomputer. Therefore, if combined with a sensor that detects birds and pests, and can shoot water or small objects at the target when pests approach, it may be possible to protect crops such as fruits from birds and pests in the future.

Innovative levitated 3D hybrid manufacturing system:

Micro-hybrid manufacturing technology including additive manufacturing[43] and aerosol jet printing[44] has become increasingly important in recent years. In particular, containerless manufacturing technology using levitation technology[45] is attractive because it avoids unwanted interactions between the container and the material[46] and contamination; e.g., acoustic levitation technology[47,48] has been widely used in many areas. For example, Cao *et al.*[49] reported rapid crystallization from acoustically levitated droplets, while Basu *et al.*[50] reported that hollow structures with unique morphology can form due to particle agglomeration in acoustically levitated nanofluid droplets. However, the technology to assemble small parts in the air is not enough. In particular, there is a lack of technology to attach materials (parts) from all directions to an object floating in the air. Thus, by combining with levitation technology, our object-shooting technology may open a new way to assemble small parts in the air for hybrid manufacturing technology in the future.

V. CONCLUSION

In conclusion, we have proposed a solid object launcher using explosive vaporization due to electrical discharge in water and examined the performance. In particular, (1) by using electrical discharge with bubble expansion, we have first succeeded in the high-speed ejection of a large volume of water of the order of 100 mm^3. (2) By using a high-speed jet of a large volume of water, we have first succeeded in launching a small object (0.92–340 mg) into the air with high speed up to ∼5 m/s. Specifically, we have demonstrated that (3) by the electrical discharge in the trapezoid chamber, an L-shaped piece of paper with $m_p = 0.92$ mg mass can be launched with an initial velocity ∼4 m/s in the direction of an elevation angle $\theta_2 \simeq 50°$, while a paper airplane with $m_p = 29.6$ mg mass can be launched with the maximum velocity ∼2 m/s along a glass slide runway with an elevation angle $\theta_1 = 45°$. (4) By the electrical discharge in the U-shaped tube chamber, a PVC plate of $m_p = 60$–340 mg mass can be launched in the vertically upward direction approximately to the height of 2–10 cm with the potential energy of $E_z \simeq 46$ μJ. Moreover, for the U-shaped tube launching device, we experimentally find that (5) the initial velocity $U_{p,0}$ of the solid object decreases with m_p and H_5, while the initial velocity $U_{l,0}$ of liquid without any solid present decreases with H_5. In addition, by the additional experiment, (6) we have clarified the importance of water-repellent treatment of the solid surface as a central design concept peculiar to solid launching devices using water ejection by the electric discharge.

ACKNOWLEDGMENTS

This work was supported by JSPS KAKENHI Grant No. JP21K18698.

AUTHOR DECLARATIONS

Conflict of Interest

The authors have no conflicts to disclose.

Author Contributions

Hideyuki Sugioka: Conceptualization (lead); Funding acquisition (lead); Methodology (equal); Software (equal); Visualization (equal); Writing – original draft (lead); Writing – review & editing (lead). **Katsuaki Murata:** Conceptualization (supporting); Data curation (lead); Formal analysis (lead); Investigation (lead); Methodology (equal); Software (lead); Visualization (lead). **Yuki Arai:** Conceptualization (supporting); Data curation (equal); Formal analysis (equal); Investigation (equal); Methodology (equal); Visualization (equal).

DATA AVAILABILITY

The data that support the findings of this study are available within the article.

REFERENCES

[1]K. Y. Ma, P. Chirarattananon, S. B. Fuller, and R. J. Wood, "Controlled flight of a biologically inspired, insect-scale robot," Science **340**, 603 (2013).
[2]Y. Chen, H. Zhao, J. Mao, P. Chirarattananon, E. F. Helbling, N.-S. P. Hyun, D. R. Clarke, and R. J. Wood, "Controlled flight of a microrobot powered by soft artificial muscles," Nature **575**, 324 (2019).
[3]S. Li, Y. Zhang, and J. Liu, "Seed ejection mechanism in an Oxalis species," Sci. Rep. **10**, 8855 (2020).
[4]N. N. Watkins, E. S. Elton, P. H. Paul, V. A. Beck, J. R. Jeffries, and A. J. Pascall, "Experimentally probing the extremes of droplet-on-demand printability via liquid metals," Phys. Fluids **33**, 121708 (2021).
[5]Y. Liu and B. Derby, "Experimental study of the parameters for stable drop-on-demand inkjet performance," Phys. Fluids **31**, 032004 (2019).
[6]M. Shigeta, "Modeling and simulation of a turbulent-like thermal plasma jet for nanopowder production," IEEJ Trans. Electr. Electron. Eng. **14**, 16 (2019).
[7]A. Asai, T. Hara, and I. Endo, "One-dimensional model of bubble growth and liquid flow in bubble jet printers," Jpn. J. Appl. Phys., Part 1 **26**, 1794 (1987).
[8]C. Cao, X. Ma, J. Xu, H. Li, and G. Liu, "Explosive boiling induced fast transportation of Leidenfrost droplet to target location," Phys. Fluids **34**, 053322 (2022).
[9]G. Wang and Z.-C. Hu, "Explosive breakup and evolution of the thermal boundary layer around a pulse-heated microwire in sub- and supercritical CO_2," Phys. Fluids **34**, 083318 (2022).
[10]H. Sugioka, S. Segawa, and M. Kubota, "High-speed side-shooter using Leidenfrost phenomena," J. Appl. Phys. **125**, 134502 (2019).
[11]H. Sugioka and A. Miyauchi, "Generation of a net flow due to fixed oblique beam structures in the nucleate boiling region," Phys. Fluids **35**, 024102 (2023).
[12]M. A. Shah, D.-G. Lee, B.-Y. Lee, and S. Hur, "Classifications and applications of inkjet printing technology: A review," IEEE Access **9**, 140079 (2021).
[13]N. K. Singh and B. Premachandran, "Saturated film boiling over a circular cylinder subjected to horizontal cross-flow in the mixed regime," Phys. Fluids **31**, 082109 (2019).

[14]S. M. Thamil Kumaran and B. Premachandran, "Study of flow and heat transfer characteristics of saturated flow film boiling over two inline cylinders," Phys. Fluids **34**, 112123 (2022).
[15]A. Asai, "Bubble dynamics in boiling under high heat flux pulse heating," J. Heat Transfer **113**, 973 (1991).
[16]K. D. Bae, S. S. Baek, H. T. Lim, K. Kuk, and K. C. Ro, "Development of the new thermal inkjet head on SOI wafer," Microelectron. Eng. **78–79**, 158 (2005).
[17]S. Sohrabi and Y. Liu, "Modeling thermal inkjet and cell printing process using modified pseudopotential and thermal lattice Boltzmann methods," Phys. Rev. E **97**, 033105 (2018).
[18]A. Khorram and S. Mortazavi, "Direct numerical simulation of film boiling on a horizontal periodic surface in three dimensions using front tracking," Phys. Fluids **34**, 052117 (2022).
[19]D. Li, H. Li, G. Yang, J. Wang, B. Huang, X. Wu, Q. Sun, C. Ma, Y. Liu, and Y. Zhang, "Subharmonic resonance and antiresonance characteristics for high-frequency confined interface vibration inkjet printing," Phys. Fluids **34**, 032104 (2022).
[20]H. Wang and Y. Hasegawa, "Multi-objective optimization of actuation waveform for high-precision drop-on-demand inkjet printing," Phys. Fluids **35**, 013318 (2023).
[21]J. Karthikeyan, C. Berndt, J. Tikkanen, S. Reddy, and H. Her, "Plasma spray synthesis of nanomaterial powders and deposits," Mater. Sci. Eng., A **238**, 275 (1997).
[22]M. J. Nicol, T. R. Brubaker, B. J. Honish, A. N. Simmons, A. Kazemi, M. A. Geissel, C. T. Whalen, C. A. Siedlecki, S. G. Bilén, S. D. Knecht, and G. S. Kirimanjeswara, "Antibacterial effects of low-temperature plasma generated by atmospheric-pressure plasma jet are mediated by reactive oxygen species," Sci. Rep. **10**, 3066 (2020).
[23]I. Zhirkov, A. Petruhins, P. Polcik, S. Kolozsvári, and J. Rosen, "Generation of super-size macroparticles in a direct current vacuum arc discharge from a Mo-Cu cathode," Appl. Phys. Lett. **108**, 054103 (2016).
[24]H. Akiyama and M. Akiyama, "Pulsed discharge plasmas in contact with water and their applications," IEEJ Trans. Electr. Electron. Eng. **16**, 6 (2021).
[25]H. Zeghioud, P. Nguyen-Tri, L. Khezami, A. Amrane, and A. A. Assadi, "Review on discharge plasma for water treatment: Mechanism, reactor geometries, active species and combined processes," J. Water Process Eng. **38**, 101664 (2020).
[26]B. K. Zuev, V. V. Yagov, and A. S. Grachev, "Discharge on boiling in a channel: Effect of channel geometry on the performance characteristics of determining metals in a liquid flow by atomic emission spectrometry," J. Anal. Chem. **61**, 1172 (2006).
[27]J. Zeleny, "The electrical discharge from liquid points, and a hydrostatic method of measuring the electric intensity at their surfaces," Phys. Rev. **3**, 69 (1914).
[28]N. Sano, H. Wang, I. Alexandrou, M. Chhowalla, K. B. K. Teo, G. A. J. Amaratunga, and K. Iimura, "Properties of carbon onions produced by an arc discharge in water," J. Appl. Phys. **92**, 2783 (2002).
[29]A. Starikovskiy, Y. Yang, Y. I. Cho, and A. Fridman, "Non-equilibrium plasma in liquid water: Dynamics of generation and quenching," Plasma Sources Sci. Technol. **20**, 024003 (2011).
[30]X. Gao, H. Chen, Q. Nie, and H. Fang, "Stability of line shapes in inkjet printing at low substrate speeds," Phys. Fluids **34**, 032002 (2022).
[31]S. Gao, Z. Liu, X. Wang, Y. Pang, Y. Ren, S. Zhao, N. Zheng, and F. Cai, "Stabilization formation characterization of metal single droplet by pneumatic drop-on-demand," Phys. Fluids **34**, 122010 (2022).
[32]X. Chen, A. P. O'Mahony, and T. Barber, "Experimental study of the stable droplet formation process during micro-valve-based three-dimensional bio-printing," Phys. Fluids **35**, 011903 (2023).
[33]V. Sukhotskiy, K. Tawil, and E. Einarsson, "Printability regimes of pure metals using contactless magnetohydrodynamic drop-on-demand actuation," Phys. Fluids **33**, 053303 (2021).
[34]Y. Guan, M. Wang, S. Wu, Y. Sha, Y. Tian, D. Ye, and Y. Huang, "The internal flow behaviors during Taylor cone formation of pulsating electrohydrodynamic jet printing," Phys. Fluids **34**, 122007 (2022).
[35]S.-H. Kang, S. Kim, D. K. Sohn, and H. S. Ko, "Analysis of drop-on-demand piezo inkjet performance," Phys. Fluids **32**, 022007 (2020).
[36]S. Buogo and G. B. Cannelli, "Implosion of an underwater spark-generated bubble and acoustic energy evaluation using the Rayleigh model," J. Acoust. Soc. Am. **111**, 2594 (2002).
[37]B. H. T. Goh, Y. D. A. Oh, E. Klaseboer, S. W. Ohl, and B. C. Khoo, "A low-voltage spark-discharge method for generation of consistent oscillating bubbles," Rev. Sci. Instrum. **84**, 014705 (2013).
[38]K. Vokurka and J. Plocek, "Experimental study of the thermal behavior of spark generated bubbles in water," Exp. Therm. Fluid Sci. **51**, 84 (2013).
[39]X. Yao, K. Guo, Y. Chen, and X. Cui, "A new experimental methodology to assess the wall pressure generated by a high-voltage underwater Spark-generated bubble," Results Phys. **12**, 571 (2019).
[40]G. O. Brown, "The history of the Darcy–Weisbach equation for pipe flow resistance," in *Environmental and Water Resources History: Proceedings and Invited Papers for the ASCE 150th Anniversary (1852-2002), Washington, DC, 3-7 November 2002* (American Society of Civil Engineers, 2003); available at https://books.google.co.jp/books/about/Environmental_and_Water_Resources_Histor.html?id=ogJSAAAAMAAJ&redir_esc=y.
[41]S. Mouden, K. F. Sarmiento, P. G. Klinkhamer, and K. A. Leiss, "Integrated pest management in western flower thrips: Past, present and future," Pest Manage. Sci. **73**, 813 (2017).
[42]M. E. Shave, S. A. Shwiff, J. L. Elser, and C. A. Lindell, "Falcons using orchard nest boxes reduce fruit-eating bird abundances and provide economic benefits for a fruit-growing region," J. Appl. Ecol. **55**, 2451 (2018).
[43]A. A. Krimpenis and G. D. Noeas, "Application of hybrid manufacturing processes in microfabrication," J. Manuf. Processes **80**, 328 (2022).
[44]N. J. Wilkinson, M. A. A. Smith, R. W. Kay, and R. A. Harris, "A review of aerosol jet printing—A non-traditional hybrid process for micro-manufacturing," Int. J. Adv. Manuf. Technol. **105**, 4599 (2019).
[45]E. H. Brandt, "Levitation in physics," Science **243**, 349 (1989).
[46]C. A. Rey, D. R. Merkley, G. R. Hammarlund, and T. J. Danley, "Acoustic levitation technique for containerless processing at high temperatures in space," Metall. Mater. Trans. A **19**, 2619 (1988).
[47]M. A. B. Andrade, A. L. Bernassau, and J. C. Adamowski, "Acoustic levitation of a large solid sphere," Appl. Phys. Lett. **109**, 044101 (2016).
[48]D. Zang, K. Lin, L. Li, Z. Chen, X. Li, and X. Geng, "Acoustic levitation of soap bubbles in air: Beyond the half-wavelength limit of sound," Appl. Phys. Lett. **110**, 121602 (2017).
[49]H.-L. Cao, D.-C. Yin, Y.-Z. Guo, X.-L. Ma, J. He, W.-H. Guo, X.-Z. Xie, and B.-R. Zhou, "Rapid crystallization from acoustically levitated droplets," J. Acoust. Soc. Am. **131**, 3164 (2012).
[50]S. Basu, E. Tijerino, and R. Kumar, "Insight into morphology changes of nanoparticle laden droplets in acoustic field," Appl. Phys. Lett. **102**, 141602 (2013).